Original Article

Capability of P- and S-wave seismic refraction in delineating the Blang Bintang Sanitary Landfill (TPA) ground subsurface

Muhammad Syukri[1*], Rosli Saad[2], and Zul Fadhli[3]

[1] *Geophysics Section, Department of Physics, Faculty of Sciences,*
Syiah Kuala University, Banda Aceh, Aceh, 23111 Indonesia

[2] *School of Physics, Universiti Sains Malaysia, Minden, Penang, 11800 Malaysia*

[3] *Department of Geophysics Engineering, Faculty of Engineering,*
Syiah Kuala University, Banda Aceh, Aceh, 23111 Indonesia

Abstract

The study was conducted at the Blang Bintang Sanitary Landfill in Aceh, Indonesia using P- and S-wave seismic refraction methods. The aim was to investigate the ground subsurface lithology. Arrival time against distance was plotted for P- and S-wave seismic refraction. Two ground subsurface boundaries were identified with three layers: top soil, highly weathered/weathered bedrock, and bedrock with Vp and Vs values of 480–730 m/s and 256–342 m/s, 1627–2010 m/s and 525–691 m/s, and 2500–3588 m/s and 836–840 m/s, respectively. The plots were also capable of indicating a fractured/fault zone with Vp and Vs values of 480–730 m/s and 256–691 m/s, respectively. Seismic refraction tomography of the P- and S-waves are capable of classifying the ground subsurface into four types of lithology: top soil, highly weathered bedrock, weathered bedrock, and bedrock with Vp and Vs values of <720 m/s and <450 m/s, 720–1620 m/s and 450–650 m/s, 1620–2800 m/s and 650–840 m/s, and >2800 m/s and >840 m/s, respectively. The fractured/fault and landfill zones were identified by seismic refraction tomography with Vp and Vs values of <720 m/s and <450 m/s, respectively. The seismic refraction of Vp and Vs have their own strengths because each of them considers different types of moduli and different velocity calculations.

Keywords: P- and S-wave seismic refraction, sediment characteristic, ground subsurface materials, investigation depth

1. Introduction

Ground subsurface characteristics are the first to study before any engineering and environment projects take place. The drilling process and the results may be affected by the ground subsurface characteristic such as water level and boulders (Timmons, 1995). To overcome such problems, geophysical methods are needed for ground subsurface studies (Auton, 1992; Barnett & Ellefsen, 2000; Crimes *et al.,* 1994; Ellefsen & Barnett, 2001; Jacobson, 1955; Jol, Parry, &

Smith, 1998; Middleton, 1977; Odum & Miller, 1988; Saarenketo & Maijala, 1994; Singhroy & Barnett, 1984; Wilcox, 1944). Ellefsen, Lucius, and Fitterman (1998, 1999) studied and evaluated ground subsurface characteristics using electrical resistivity sounding, time domain electromagnetic sounding, frequency domain electromagnetic profiling, and ground-penetrating radar. Spectral analysis of surface waves or refraction microtremor is applied to evaluate the subsurface profile using velocity reversal (Louie, 2001). The application of the surface wave only resolves the S-wave into 1-dimensional vertical profiles with low resolution while the real situations are non-unique and need high resolution profiles.

The seismic refraction method effectively enhances a shallow subsurface profile for geotechnical engineering

*Corresponding author
Email address: m.syukri@unsyiah.ac.id; rosli@usm.my

applications. Elastic moduli and the strength of geological materials are related to seismic compressional wave (P-wave) and shear wave (S-wave) velocities. Seismic refraction is an effective tool for horizontal and lateral characterization as well as vertical characterization. The P-wave seismic refraction method is generally applied for a subsurface study, such as transportation, excavation, and material characterization profiles, for geotechnical work (Rucker, 2000; Yord-kayhun, 2011). The P-wave seismic refraction method works only when the wave velocity increases with depth. The S-wave seismic refraction method is applied for studies of dynamic parameters of geological materials (Viksne, 1976) but it also has the same limitations as the P-wave refraction method. The advantages of the S-wave seismic refraction method over other geophysical methods in studying the ground subsurface include better spatial resolution and the results behave the same in saturated or unsaturated areas (McLamore, Anderson, & Espana, 1978). Clays are often prevalent in soils along with depositional lenses within sediments. Generally, these affect S-waves less than they affect electrical conductivity, electrical resistivity sounding, time domain electromagnetic sounding, and ground-penetrating radar.

The weaknesses of P-wave seismic refraction method can be strengthened by the S-wave seismic refraction method and vice versa. Performing both P- and S-wave seismic refraction methods on the same line using the same equipment and geophone array provide comprehensive shallow subsurface characterization rather than using only one method of either P-wave or S-wave. A seismic refraction study was conducted at Blang Bintang Sanitary Landfill (*Tempat Pemrosesan Akhir*) in Aceh, Indonesia. The aim was to investigate the ground subsurface profile using P- and S-wave seismic refraction. The study was conducted on the same spread line using a special setting which was permitted in each method.

2. General Geology of the Study Area

The study area was located at the new Blang Bintang Sanitary Landfill in Aceh, Indonesia with latitude and longitude coordinates of 5.517303° and 95.473800°, respectively (Figure 1). The study area was located at the eastern part of Sultan Iskandar Muda International Airport, Aceh and in the south-west part of Kuede town with distances of about 6 km and 8.2 km, respectively. Banda Aceh city is located at the western part of the study area with a distance of about 18.5 km. The study area is isolated and located in a highland area with an elevation of 145–172 m.

Aceh consists of four major volcano-sedimentary sequences which are separated by unconformities that are pre-Tertiary in age and Tertiary to Recent (Syukri & Saad, 2017). The Lam Tuba volcanic dominated Banda Aceh Quadrangle and Krueng Raya consist of andesitic to dacitic volcanics, pumiceous breccia, tuffs, agglomerates, and ash flows (Figure 2). The Seulimeum formation is intruded by ash composed of tuffaceous and calcareous sandstones, conglomerates, and minor mudstones (Bennett *et al.,* 1981). The Barisan range runs from Aceh to Lampung through the middle of Sumatra Island and consists of flat and low alluvial areas including flat-topped hills within the range while a continuous axial valley system follows closely to the Barisan range crest as an outcrop of the main fault line (Sumatran fault system).

3. Methodology

Two spread lines (P and S) were designed on the same line at the study area to perform the P- and S-wave seismic refraction method using 24-channel seismograph

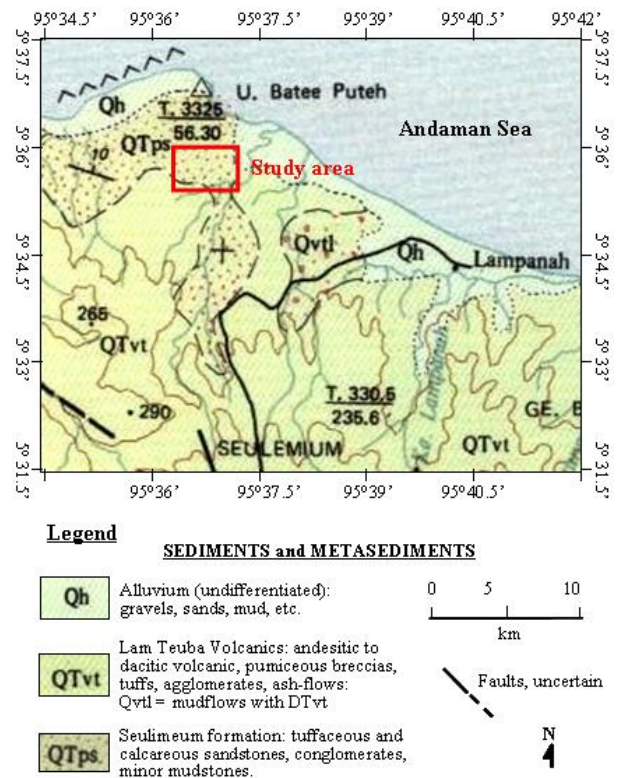Figure 1. Study area at Blang Bintang Sanitary Landfill, Aceh, Indonesia (Google Earth, 2016).

Figure 2. Geology of the study area (Modified from Bennett *et al.,* 1981).

(Terraloc MK8, ABEM Instrument, AB, Sweden) (Figure 3). Each spread line was designed using 4 m geophones spacing to accommodate 28 Hz vertical geophones and 10 Hz horizontal geophones for the P- and S-wave methods, respectively, with a total length of each spread line of 92 m.

The P-wave seismic refraction method used a total of 24 vertical geophones with a natural frequency of 28 Hz and 6 kg sledgehammer seismic source to strike vertically on a metal plate to produce the P-wave. A total of 9 shot locations were chosen and the seismic signals are recorded for each shot position for processing. Meanwhile the S-wave seismic refraction method used a total of 24 horizontal geophones with a natural frequency of 10 Hz and striking a 6 kg sledgehammer horizontally on both sides of a wooden plank which was weighted at the top to provide a good friction contact with the ground surface to produce the S-wave (Figure 4). A total of 3 shot locations were chosen and the seismic signals are recorded for each shot position and direction for processing. Table 1 shows the details of the setup of the spread lines including shot locations for the P- and S-wave seismic refraction methods. Figure 5 shows the relationship of the P and S lines including shot locations.

The P- and S-wave data were filtered using IXRefract software to enhance the signals. The P-wave refraction arrival times were picked using Firstpix software. The S-wave seismic refraction data were processed using Microsoft Excel and Surfer 10 software for picking the arrival time. The tomography profile for the P- and S-wave seismic refraction methods were produced using SeisOpt@2D software for validation and interpretation (White, 1989).

4. Results and Discussion

The P- and S-wave arrival times were picked using special techniques and software. The arrival times were plotted against geophone distance for velocity analysis and tomography processing. Figure 6 shows the first arrival time of the P-wave seismic signal of 24 traces with the shot point

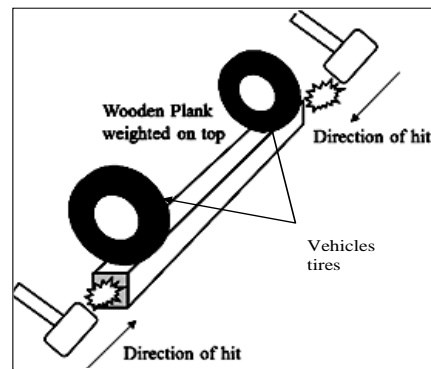Figure 3. The P- and S-wave spread lines at the study area (Google Earth, 2016).

Figure 4. S-wave seismic refraction hammering techniques.

Table 1. Line setup and shot locations for P- and S-wave seismic refraction methods.

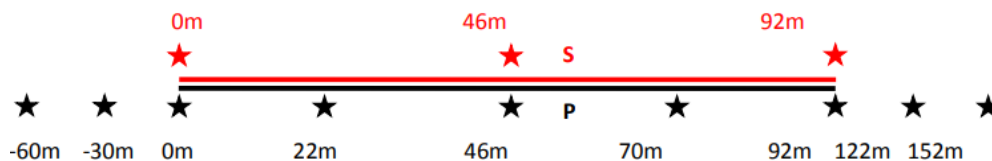|	P-wave refraction				S-wave refraction		
Spread name	Location (m)	Latitude Longitude (°)	Shot location (m)	Spread name	Location (m)	Latitude Longitude (°)	Shot location (m)
P	0	5.517536 95.476951	–60, –30, 0, 22, 46, 70, 92, 122,	S	0	5.517536 95.476951	0, 46, 96
	92	5.518292 95.477268	152		92	5.518292 95.477268	

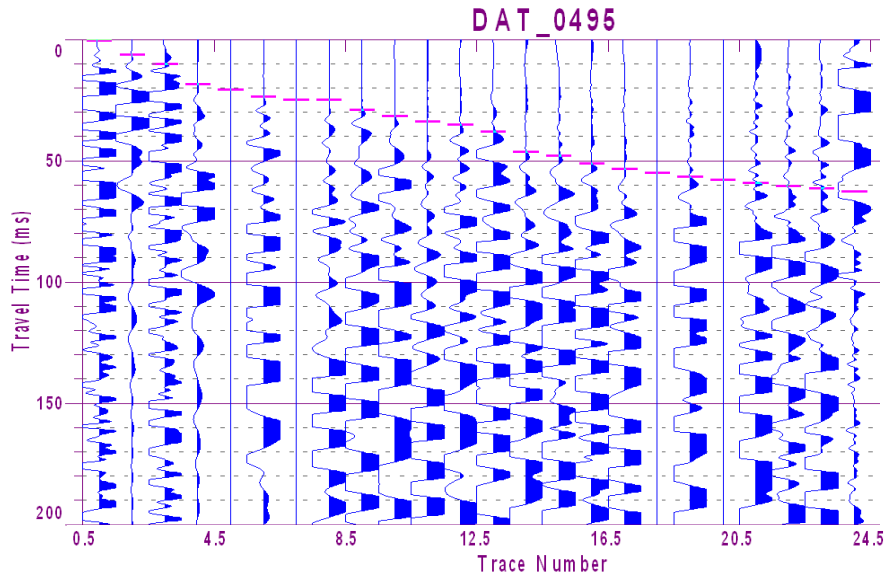Figure 5. Correlation between spread lines, P and S together with shot locations.

Figure 6.   First arrival pick of P-wave seismic signal with a shot located at 0 m.

located at 0 m and Figure 7 shows first arrival time of the S-wave seismic signal with shot point located at 46 m.

Figure 8 shows the plot of the first arrival times against geophone distance for the P-wave seismic refraction with the appropriate shot points for velocity analysis. The plot shows the survey line that consists of the three-layer case. The first layer was identified by the velocity value of 480–730 m/s, interpreted as top soil with the effect of a fracture/fault identified at 80–85 m. The second layer was identified by a velocity value of 1627–2010 m/s, interpreted as highly weathered/weathered bedrock with few fractures/faults identified at 25–60 m. The third layer was identified by a velocity

value of 2500–3588 m/s, interpreted as bedrock with few fractures/faults identified at 12–74 m.

The plot of the first arrival times against geophone distance for S-wave seismic refraction (Figure 9) shows that the survey line consisted of the three-layer case. The first layer was identified by a velocity value of 256–342 m/s and was interpreted as top soil. The second layer was identified by a velocity value of 525–691 m/s which was interpreted as highly weathered/weathered bedrock with few fractures/faults identified at 12–80 m, and the third layer was identified by a velocity value of 836–840 m/s which was interpreted as bedrock.
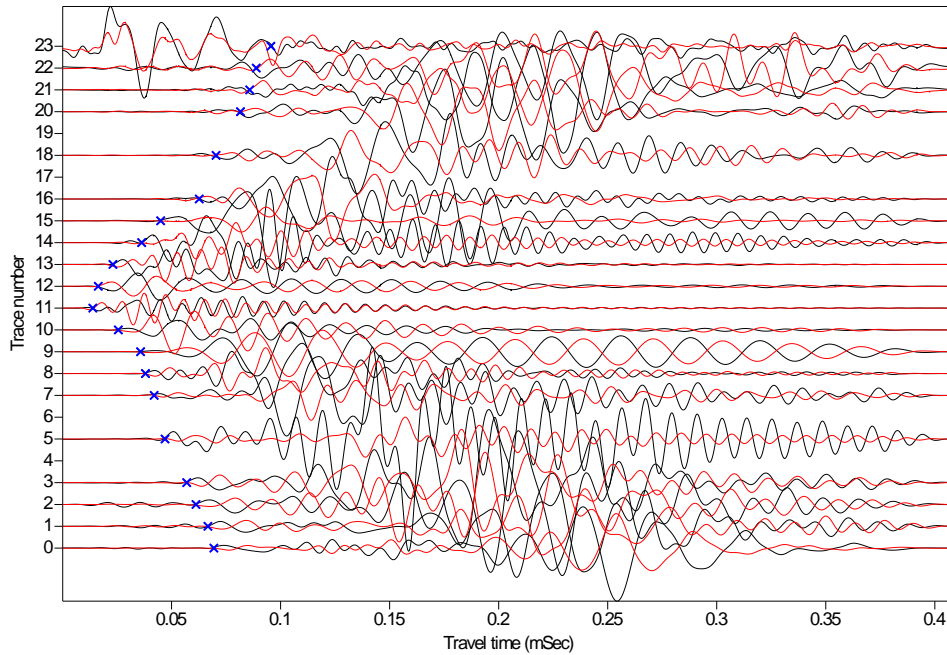

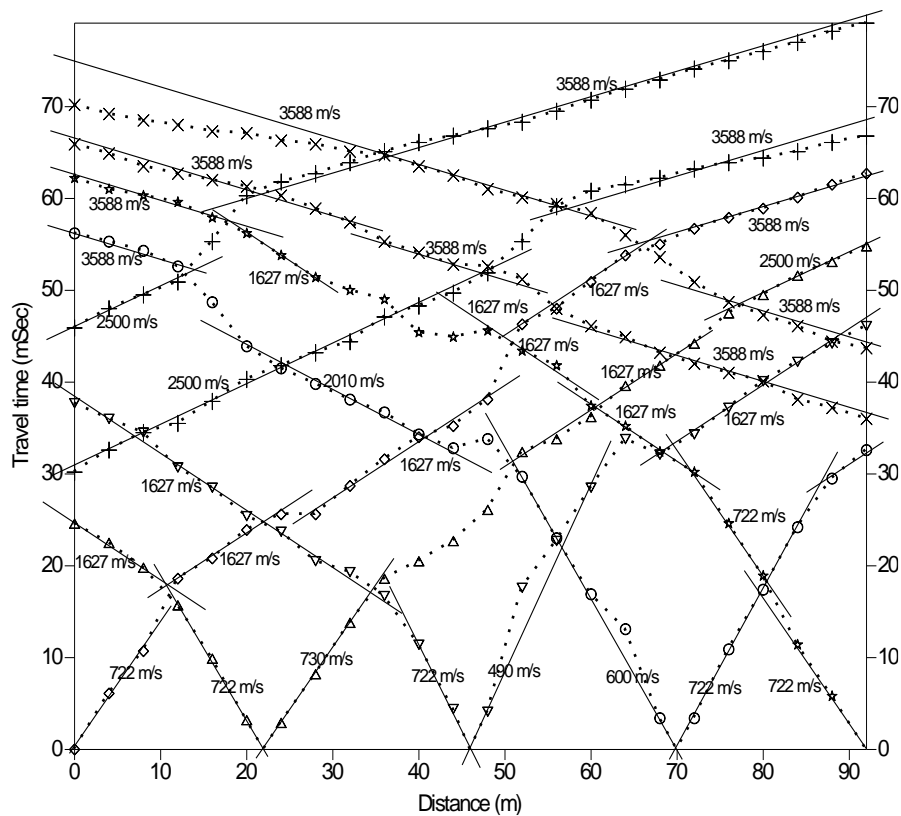Figure 7.   First arrival pick of S-wave seismic signal with shot located at 46 m.

Figure 8.   Plot of arrival time against distance for P-wave seismic refraction of line P.

Figure 10 shows the seismic refraction tomography of survey line P. Figure 10a shows the data points of the velocity distribution for the P-wave seismic refraction and Figure 10b is the P-wave velocity tomography profile. Both were identified by SeisOpt@2D software. The results showed that it consisted of a 4-layer case. The first layer (top soil) and the fracture zone were identified with velocity values <720 m/s. The fracture zone was located at a depth of 10–16m. The second layer with a velocity of 720–1620 m/s was interpreted as highly weathered bedrock identified at a depth of 0–2 m while the third layer was interpreted as weathered bedrock identified at a depth of 7–18 m which was indicated by a velocity value of 1620–2800 m/s. Finally, the fourth layer was interpreted as bedrock identified at a depth of >16 m with a velocity value of >2800 m/s.

Figure 11 shows the seismic refraction tomography of survey line S. Figure 11a shows the data points of the velocity distribution for S-wave seismic refraction and Figure 11b is the S-wave velocity tomography profile. Both were identified by SeisOpt@2D software. The results showed that it consisted of the 4-layer case. The first layer (top soil) with a thickness of 0–8 m was identified with a velocity value <450 m/s. The second layer with a velocity value of 450–650 m/s was interpreted as highly weathered bedrock identified at a depth of 0–9 m while the third layer was interpreted as weathered bedrock identified at a depth of 2–19 m which was indicated by a velocity value of 650–840 m/s. Finally, the fourth layer was interpreted as bedrock identified at >4 m depth with a velocity value >840 m/s.

Generally, the P- and S-wave seismic refraction methods produce different subsurface results since the P- and S-wave velocities are affected by different types of moduli. The plot of arrival time against distance is capable of identifying a subsurface boundary and is able to detect fractured areas since it is considered to be a bulk/shear modulus and average velocity while the Vp and Vs tomography manages to enhance the lithology including boundaries, fractured areas, and depth because it is considered to be a bulk/shear modulus and velocity distribution. Investigation of the depth of S-wave seismic refraction was the same compared to P-wave seismic refraction even though the shot distance was short because the frequency of the S-wave was lower than the P-wave and its amplitude was higher compared to the P-wave.

5. Conclusions

Both, P- and S-wave seismic refraction methods can be used to study ground subsurface lithologies. Each method enhances ground subsurface material with different types of strength. The P-wave seismic refraction considers bulk modulus while S-wave seismic refraction considers shear modulus. Each method shows different types of subsurface strength. The top soil showed a different response on the respective modulus indicated by the P- and S-wave travel time graph with velocities of 480–730 m/s and 256–691 m/s, respectively. Meanwhile, the seismic refraction tomography indicated top soil with P- and S-waves <720 m/s and <450
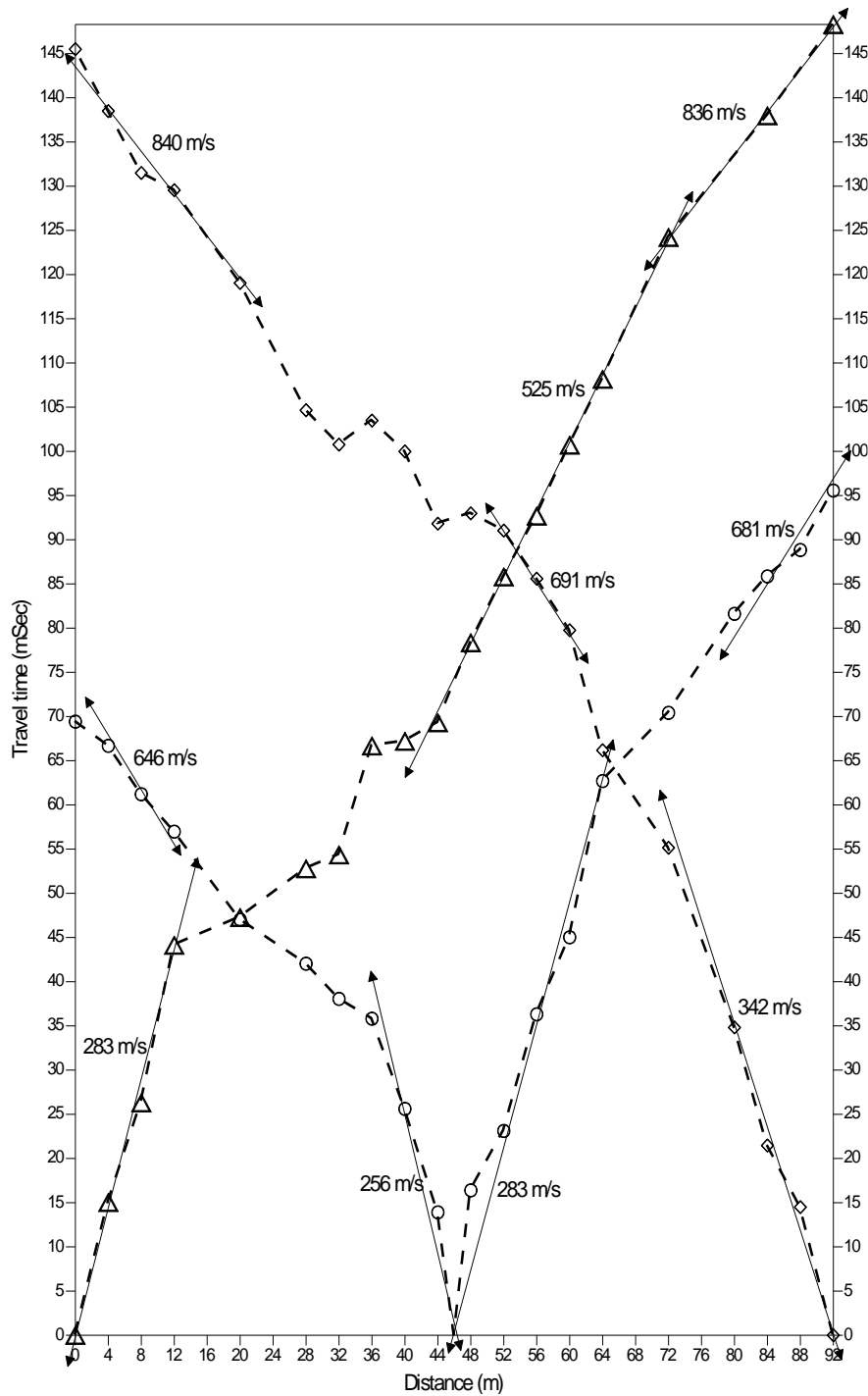
Figure 9. Plot of arrival time against distance for S-wave seismic refraction of line S.

m/s, respectively. The P- and S-wave velocities were identified within the range of soil used for landfill (reclaiming) purposes (Ellefsen & Barnett, 2001; Yordkayhun, 2011). Depth investigation using S-wave seismic refraction is greater compared to P-wave seismic refraction if the shot distance remains the same for each method. This is related to the frequency and amplitude of the waves.
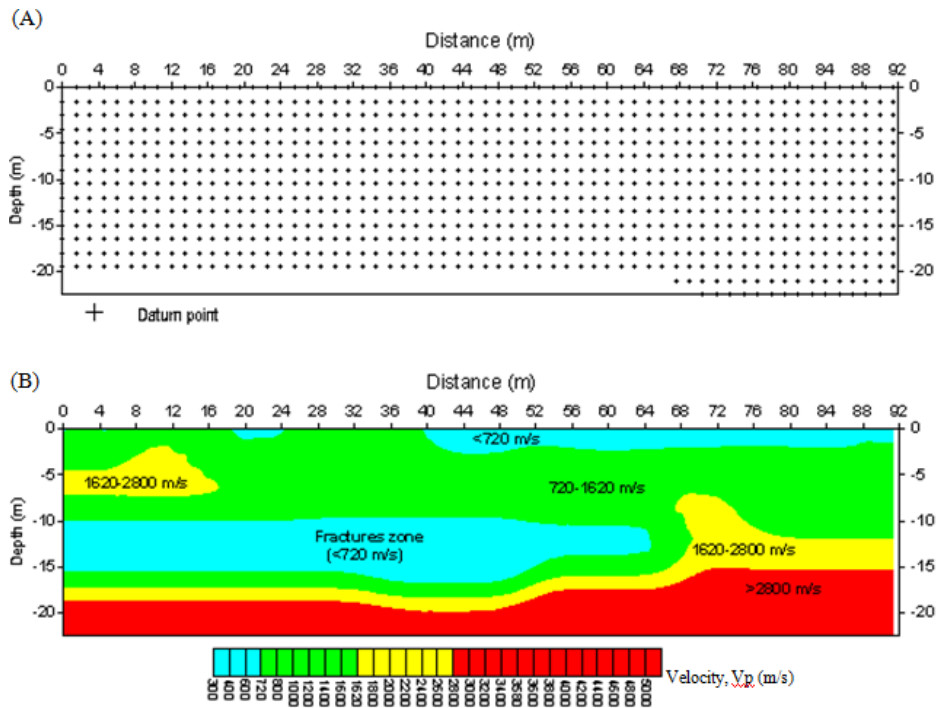
Acknowledgements

Figure 10.   P-wave seismic refraction of line P: (A) velocity data point locations and (B) P-wave velocity tomography profile.

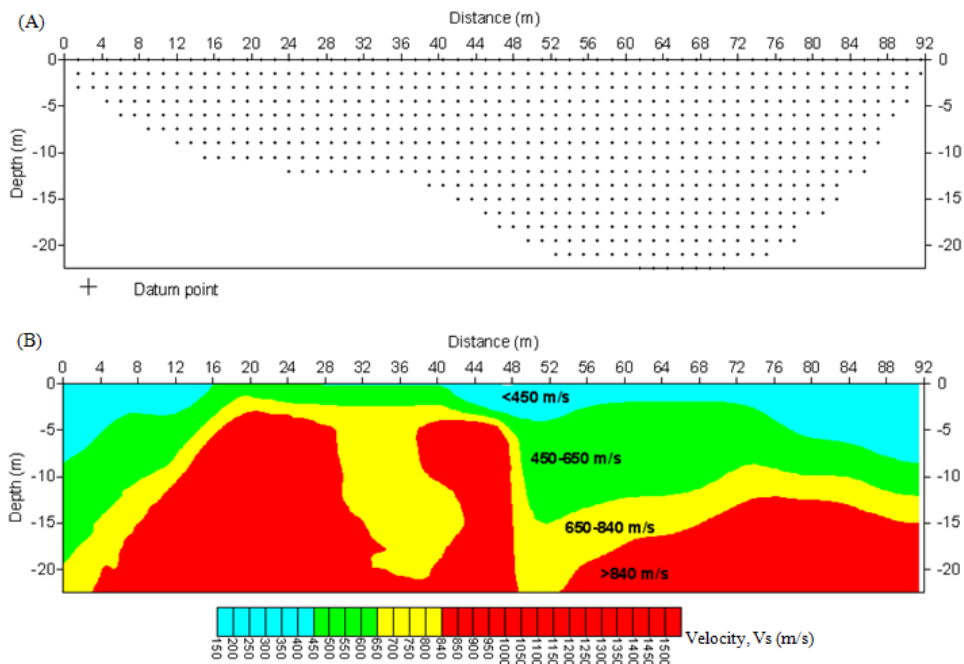Figure 11.   S-wave seismic refraction of line S: (A) velocity data point locations and (B) S-wave velocity tomography profile.

References

Auton, C. A. (1992). The utility of conductivity surveying and resistivity sounding in evaluating sand and gravel

deposits and mapping drift sequences in northeast Scotland. *Engineering Geology*, *32*, 11–28.

Barnett, A., & Ellefsen, K. J. (2000). Assessment of the alluvial sediments in the Big Thompson River valley, Colorado. U.S. Geological Survey Digital Data Series, DDS-066. Retrieved from https://pubs.usgs.gov/dds/dds-066/

Bennett, J. D., McC Jeffrey, D., Bridge, D., Cameron, N. R., Djunuddin, A., Ghazali, S. A. & Whandoyo, R. (1981). *Geologic map of the Banda Aceh Quadrangle*. Indonesia Geological Research and Development Center, Sumatra, Indonesia.

Crimes, T. P., Chester, D. K., Hunt, N. C., Lucas, G. R., Mussett, A. E., Thomas, G. S. P., & Thompson, A. (1994). Techniques used in aggregate resource analysis of four areas of the UK. *Quarterly Journal of Engineering Geology*, *27*(2), 165–192.

Ellefsen, K. J., Lucius, J. E., & Fitterman, D. V. (1998). *An evaluation of several geophysical methods for characterizing sand and gravel deposits* (Report 98-221). Retrieved from https://pubs.er.usgs.gov/publication/ofr98221

Ellefsen, K. J., Lucius, J. E., & Fitterman, D. V. (1999). Geophysics in exploration for sand and gravel. *Proceedings, 34th Forum on the Geology of Industrial Minerals 102,* 147–149.

Ellefsen, K. J., & Barnett, A. (2001). An investigation of alluvial sediments using S-wave refraction: A case study. *Proceedings of the Symposium on the Application of Geophysics to Engineering and Environmental Problems*, Denver, CO.

Google Earth. (2016). Retrieved from https://www.google.co.th/intl/th/earth/

Jacobson, R. P. (1955). Geophysical case history of a commercial gravel deposit. *Mining Engineering, 7,* 158–162.

Jol, H. M., Parry, D., & Smith, D. G. (1998). Ground penetrating radar: Applications in sand and gravel exploration. In P. T. Bobrowsky (Ed.), *Aggregate resources: A global perspective* (pp. 295–306). Rotterdam, Netherlands: A.A. Balkema.

Louie, J. L. (2001). Faster, Better, Shear-wave velocity to 100 meters depth from refraction microtremor arrays. *Bulletin of the Seismological Society of America, 91*, 347-364.

McLamore, V. R., Anderson, D. G., & Espana, C. (1978). Crosshole testing using explosive and mechanical energy sources STP 654. *American Society for Testing and Materials, 30*–55.

Middleton, R. S. (1977). Ground and airborne geophysical studies of sand and gravel in the Toronto region. *Ontario Geological Survey Study GS18*. Retrieved from http://www.geologyontario.mndmf.gov.on.ca/mndm files/pub/data/imaging/S018/S018.pdf

Odum, J. K., & Miller, C. H. (1988). Geomorphic, seismic, and geotechnical evaluation of sand and gravel deposits in the Sheridan, Wyoming, area: *U.S. Geological Survey Bulletin 1845*. Washington D.C: Government Printing Office.

Rucker, M. L. (2000). Applying the seismic refraction technique to exploration for transportation facilities. *1st International Conference on the Application of Geophysical Methodologies to Transportation Facilities and Infrastructure*. St. Louis, MO.

Saarenketo, T., & Maijala, P. (1994). Applications of geophysical methods to sand, gravel and hard rock aggregate prospecting in northern Finland. In G. W. Lüttig (Ed.), *Aggregates—Raw Materials Giant: Report on the 2nd International Aggregates Symposium* (pp. 109–123). Erlangen, Germany.

Singhroy, V. H., & Barnett, P. J. (1984). Locating subsurface mineral aggregate deposits from airborne infrared imagery (reflected and thermal): A case study in southern Ontario. *Proceedings of the International Symposium on Remote Sensing of Environment, 3rd Thematic Conference: Remote Sensing for Exploration Geology*, 523–539.

Syukri, M., & Saad, R. (2017). Seulimeum segment characteristic indicated by 2-D resistivity imaging method. *NRIAG Journal of Astronomy and Geophysics, 6*(1), 210-217.

Timmons, B. J. (1995). Prospecting for natural aggregates: An update. *Rock Products, 98*(1), 31–37.

Viksne, A. (1976). *Evaluation of in situ shear wave velocity measurement techniques* (No. REC-ERC-76-6). Division of Design, Engineering and Research Center, U.S. Department of the Interior, Denver, CO.

White, D. J. (1989). Two-dimensional seismic refraction tomography. *Geophysical Journal International, 97* (2), 223–245.

Wilcox, S. W. (1944). Sand and gravel prospecting by the earth resistivity method. *Geophysics, 9,* 36–46.

Yordkayhun, S. (2011). Detecting near-surface objects with seismic travel time tomography: Experimentation at a test site. *Songklanakarin Journal of Science and Technology, 33*(4), 477–485.